

## Theory of continuum percolation. III. Low-density expansion

Alon Drory,<sup>1</sup> Brian Berkowitz,<sup>2</sup> Giorgio Parisi,<sup>1</sup> and I. Balberg<sup>3</sup>

<sup>1</sup>*Dipartimento di Fisica and INFN, Università La Sapienza, Piazzale Aldo Moro 2, Roma 00187, Italy*

<sup>2</sup>*Department of Environmental Science and Energy Research, Weizmann Institute, Rehovot 76100, Israel*

<sup>3</sup>*Department of Physics, Hebrew University, Jerusalem, Israel*

(Received 11 December 1996)

We use a mapping between the continuum percolation model and the Potts fluid (a system of interacting  $s$ -state spins which are free to move in the continuum) to derive the low-density expansion of the pair connectedness and the mean cluster size. We prove that given an adequate identification of functions, the result is equivalent to the density expansion derived from a completely different point of view by Coniglio, DeAngelis, and Forlani [J. Phys. A **10**, 1123 (1977)] to describe physical clustering in a gas. We then apply our expansion to a system of hypercubes with a hard core interaction. The calculated critical density is within approximately 5% of the results of simulations, and is thus much more precise than previous theoretical results which were based on integral equations. We suggest that this is because integral equations smooth out overly the partition function (i.e., they describe predominantly its analytical part), while our method targets instead the part which describes the phase transition (i.e., the singular part). [S1063-651X(97)07107-9]

PACS number(s): 64.60.Ak

### I. INTRODUCTION

Two previous papers in this series [1], hereafter referred to as I and II, presented a general formalism of continuum percolation [2], where the system consists of classical particles interacting through a pair potential  $v(\vec{r}_i, \vec{r}_j)$ , such that they can also bind (or connect) to each other with a probability  $p(\vec{r}_i, \vec{r}_j)$ . Such a model is useful to describe microemulsions [3], composite materials [4], or some properties of water [5]. In this model, the clustering depends on the density  $\rho$  of the particles. As the density increases, so does the mean cluster size  $S$ . At a well defined critical density  $\rho_c$ ,  $S$  diverges, which signals the appearance of an infinite cluster. This is the percolation phase transition. Its critical behavior (i.e., the critical exponents) seem to be identical to the behavior of lattice percolation (see, however, a recent work by Okazaki *et al.* [6] which claims differently) but the percolation threshold—the critical density—is sensitive to all the details of the system.

The early theoretical attempts to calculate the percolation threshold culminated with the introduction by Balberg *et al.* of the notion of a critical total excluded volume  $B_c$  [7]. The excluded volume is the volume around one particle of the system in which the center of a second particle must be in order for the two particles to be connected. The total excluded volume of the system is therefore another measure of the number of particles in the system, i.e., of the density. When measured in this way, the numerical value of the percolation threshold seemed to be relatively insensitive to the shape of the particles (unlike the density itself). It was therefore considered an approximately universal quantity. However, this concept could not take into account other properties of the system, such as interactions between the particles, nor could it explain the remaining dependence of the percolation threshold on the details of the system.

In 1977, Coniglio, DeAngelis, and Forlani proposed a different approach, based on a density expansion of the mean cluster size [8]. This in turn served as the basis of an ap-

proximate calculation based on some integral equations analogous to those encountered in the theory of liquids [9]. This approach yielded finally a theoretical prediction of the percolation threshold, but the results remained only qualitative, discrepancies of up to 40% with computer simulations being common [10,11].

Recently, however, Alon, Drory, and Balberg [12] and Drory *et al.* [13] obtained quantitatively adequate results from the expansion of Coniglio, DeAngelis, and Forlani, by using the density expansion directly instead of integral equations. This posed a curious problem, because the critical density is not low enough to suggest that a power expansion should work. On the other hand, the expansion of Coniglio, DeAngelis, and Forlani had been developed to describe physical clustering in a gas, and its extension to general continuum percolation models was based on extensive analogies. It seemed that a more solid theoretical foundation was needed for continuum percolation before this puzzle could be addressed. Such a foundation has been laid in I and II, and we can now treat the problem of density expansions from a fresh point of view. The formalism presented in I and II is based on a quantitative mapping between the percolation model and an extension of the Potts model, the Potts fluid. We have only recently learned that such a mapping had already been introduced in 1982 by Klein [14]. This was then further elaborated by Given [15], Given and Klein [16], and Given and Stell [17]. These authors used the mapping to generate a Born-Green hierarchy of equations for the  $n$ -connectedness functions (which are to percolation systems what  $n$ -correlation functions are to liquids), and from there to derive several integral equations and various bounds on, e.g., the mean cluster size. We think these results and ours should be viewed as complementary. The earlier developments of Klein, Given, and Stell were made along the lines adopted in chemical physics and the theory of liquids, i.e., mainly integral equations and  $n$ -connectedness function hierarchies. Our research, on the other hand, follows the lines adopted in the statistical mechanics theory of critical phe-

nomena, i.e., mean field theory, exact solutions of simplified models (e.g., one-dimensional systems [18]), and various perturbative expansions. The two approaches therefore complement each other to yield a comprehensive theory of continuum percolation.

For easy reference, we recall here the essential definitions and results. The  $s$ -state Potts fluid is a system of  $N$  classical spins  $\{\lambda_i\}_{i=1}^N$  interacting with each other through a spin-dependent pair potential  $V(\vec{r}_i, \lambda_i; \vec{r}_j, \lambda_j)$ , such that

$$V(\vec{r}_i, \lambda_i; \vec{r}_j, \lambda_j) \equiv V(i, j) = \begin{cases} U(\vec{r}_i, \vec{r}_j) & \text{if } \lambda_i = \lambda_j \\ W(\vec{r}_i, \vec{r}_j) & \text{if } \lambda_i \neq \lambda_j. \end{cases} \quad (1.1)$$

The spins are coupled to an external field  $h(\vec{r})$  through an interaction Hamiltonian

$$H_{\text{int}} = - \sum_{i=1}^N \psi(\lambda_i) h(\vec{r}_i), \quad (1.2)$$

where

$$\psi(\lambda) = \begin{cases} s-1 & \text{if } \lambda = 1 \\ -1 & \text{if } \lambda \neq 1. \end{cases} \quad (1.3)$$

Up to some unimportant constants, the Potts fluid partition function (more precisely, the configuration integral) is

$$Z = \frac{1}{N!} \sum_{\{\lambda_m\}} \int d\vec{r}_1 \cdots d\vec{r}_N \exp \left[ -\beta \sum_{i>j} V(i, j) + \beta \sum_{i=1}^N h(i) \psi(\lambda_i) \right]. \quad (1.4)$$

The magnetization of the Potts fluid is defined as

$$M = \frac{1}{\beta N(s-1)} \frac{\partial \ln Z}{\partial h}, \quad (1.5)$$

where  $h$  is the now constant external field. The susceptibility is

$$\chi = \frac{\partial M}{\partial h}. \quad (1.6)$$

The  $n$ -density functions of the Potts fluid are defined as

$$\begin{aligned} \rho^{(n)}(\vec{r}_1, \lambda_1; \dots; \vec{r}_n, \lambda_n) &= \frac{1}{Z(N-n)!} \int d\vec{r}_{n+1} \cdots d\vec{r}_N \\ &\times \exp \left[ -\beta \sum_{i>j} V(i, j) - \beta \sum_{i=1}^N h(i) \psi(\lambda_i) \right]. \end{aligned} \quad (1.7)$$

Of particular interest is the spin pair-distribution function  $g^{(2)}(\vec{x}, \alpha; \vec{y}, \gamma)$ , defined as

$$g^{(2)}(\vec{x}, \alpha; \vec{y}, \gamma) \equiv \frac{1}{\rho(\vec{x})\rho(\vec{y})} \rho^{(2)}(\vec{x}, \alpha; \vec{y}, \gamma), \quad (1.8)$$

which tends to 1 when  $|\vec{x} - \vec{y}| \rightarrow \infty$ . Here  $\rho(\vec{x})$  is the local numerical density. It is often useful to define a spin correlation function  $h^{(2)}(\vec{x}, \alpha; \vec{y}, \gamma)$  as

$$h^{(2)}(\vec{x}, \alpha; \vec{y}, \gamma) \equiv g_s^{(2)}(\vec{x}, \alpha; \vec{y}, \gamma) - 1. \quad (1.9)$$

This function tends to zero when  $|\vec{x} - \vec{y}| \rightarrow \infty$ .

Any continuum percolation model defined by  $v(i, j)$  and  $p(i, j)$  can be mapped onto an appropriate Potts fluid model with a pair-spin interaction defined by

$$\begin{aligned} U(i, j) &= v(i, j), \\ \exp[-\beta W(i, j)] &= q(i, j) \exp[-\beta v(i, j)], \end{aligned} \quad (1.10)$$

where

$$q(\vec{r}_i, \vec{r}_j) \equiv 1 - p(\vec{r}_i, \vec{r}_j) \quad (1.11)$$

is the probability of disconnection.

The relation between the Potts magnetization and the percolation probability  $P(\rho)$  is

$$\lim_{h \rightarrow 0} \lim_{N \rightarrow \infty} \lim_{s \rightarrow 1} M = P(\rho). \quad (1.12)$$

For densities lower than the critical density  $\rho_c$ , the susceptibility is directly related to the mean cluster size  $S$

$$\lim_{h \rightarrow 0} \lim_{N \rightarrow \infty} \lim_{s \rightarrow 1} \chi = \beta S \quad (\rho < \rho_c). \quad (1.13)$$

An important quantity in the percolation model is the pair connectedness function  $g^\dagger(\vec{x}, \vec{y})$ , the meaning of which is

$$\begin{aligned} &\rho(\vec{x})\rho(\vec{y})g^\dagger(\vec{x}, \vec{y})d\vec{x}d\vec{y} \\ &= (\text{probability of finding two particles in} \\ &\text{regions } d\vec{x} \text{ and } d\vec{y} \text{ around the positions} \\ &\vec{x} \text{ and } \vec{y}, \text{ such that they both belong} \\ &\text{to the same cluster}). \end{aligned} \quad (1.14)$$

This function is related to the mean cluster size by

$$S = 1 + \rho \int d\vec{r} g^\dagger(\vec{r}), \quad (1.15)$$

where we assume, as we usually shall, that the system is translationally invariant, so that  $g^\dagger(\vec{x}, \vec{y}) = g^\dagger(\vec{x} - \vec{y})$  and  $\rho(\vec{x}) = \rho(\vec{y}) = \rho$ .

The pair connectedness is related to the Potts pair correlation functions by

$$\begin{aligned} g^\dagger(\vec{x}, \vec{y}) &= \lim_{s \rightarrow 1} [g^{(2)}(\vec{x}, \sigma; \vec{y}, \sigma) - g^{(2)}(\vec{x}, \sigma; \vec{y}, \eta)] \\ &= \lim_{s \rightarrow 1} [h^{(2)}(\vec{x}, \sigma; \vec{y}, \sigma) - h^{(2)}(\vec{x}, \sigma; \vec{y}, \eta)], \end{aligned} \quad (1.16)$$

where the spins  $\sigma$  and  $\eta$  are arbitrary except for the conditions  $\sigma, \eta \neq 1$  and  $\sigma \neq \eta$ .

Recently, Drory has applied this formalism to a nontrivial one-dimensional model and managed to obtain its exact solution [18]. Continuing the investigation of the usefulness of this formalism, we consider in the present work the region  $\rho < \rho_c$  and derive series expansion in powers of the density for the mean cluster size and the pair connectedness (the percolation probability, on the other hand, vanishes identically for these densities). To do this we introduce in Sec. II

the spin-functional differentiation, which is a simple generalization of the usual functional differentiation. With this tool, we easily obtain a diagrammatic expansion of the relevant quantities in Sec. III. Section IV compares this expansion to the one derived by Coniglio, DeAngelis, and Forlani; from a completely different starting point [8]. Section V then applies the general results to a specific case, the extended hypercube models. The results are presented in Sec. VI. Finally in Sec. VII we discuss the reasons for the quantitative success of the present approach, compared with the inadequacy of previous analytical attempts.

## II. SPIN-FUNCTIONAL DIFFERENTIATION

The mathematical properties of the Potts fluid are very similar to the corresponding ones for a classical fluid. In the following derivations, we therefore follow very closely the presentation of Hansen and McDonald of the theory of classical fluids [9]. Occasionally we shall skip some mathematical details which are identical for the Potts fluid and for the classical one.

Since all the quantities in which we are interested are expressible as statistical averages, we may choose to work in the grand canonical ensemble rather than in the canonical one.

The grand canonical partition function  $\Xi$  is given by

$$\Xi = \sum_{N=0}^{\infty} \frac{1}{N!} \int d1 \cdots dN \sum_{\lambda_1, \dots, \lambda_N} \prod_{i=1}^N z^*(i, \lambda_i) \times \prod_{i>j}^N \exp[-\beta V(i, j)], \quad (2.1)$$

where

$$z^*(i, \lambda_i) = \left( \frac{2\pi\beta\hbar^2}{m} \right)^{3/2} \exp[\beta\mu + \beta h(i)\psi(\lambda_i)] \quad (2.2)$$

is the generalized activity. Here,  $m$  is the mass of the particles (the spins),  $\mu$  is the chemical potential, and  $\hbar$  is Planck's constant.

The  $n$ -density functions are now defined to be

$$\begin{aligned} \rho^{(n)}(\vec{r}_1, \lambda_1; \dots; \vec{r}_n, \lambda_n) \\ = \frac{1}{\Xi} \sum_{N=0}^{\infty} \frac{1}{(N-n)!} \int d\vec{r}_{n+1} \cdots d\vec{r}_N \\ \times \sum_{\lambda_{n+1}, \dots, \lambda_N} \prod_{i=1}^N z^*(i, \lambda_i) \prod_{j>i}^N \exp[-\beta V(i, j)]. \end{aligned} \quad (2.3)$$

Paper II presented a generalization of the functional derivative, which will be called hereafter the spin-functional derivative. Let  $\mathcal{F}[t(\vec{r}, \lambda)]$  be a functional of the function  $t(\vec{r}, \lambda)$ , which depends on a position variable  $\vec{r}$  as well as on an associated discrete spin variable  $\lambda$ . Then the spin-functional derivative  $\delta\mathcal{F}/\delta t$  is defined through the relation

$$\delta\mathcal{F} = \int d\vec{r} \sum_{\lambda} \frac{\delta\mathcal{F}}{\delta t(\vec{r}, \lambda)} \delta t(\vec{r}, \lambda), \quad (2.4)$$

where  $\delta\mathcal{F}$  is the change in  $\mathcal{F}$  associated with a variation  $\delta t$  in  $t(\vec{r}, \lambda)$ . The only difference with the usual functional derivative is in the added summation over the spin variable. It is easily seen that this does not change any of the basic properties of the functional derivative operator. In particular, we have (see, e.g., Hansen and McDonald [9]) that

$$\frac{\delta t(\vec{x}, \alpha)}{\delta t(\vec{y}, \gamma)} = \delta(\vec{x} - \vec{y}) \delta_{\alpha, \gamma}, \quad (2.5)$$

and

$$\frac{\delta}{\delta t(\vec{y}, \gamma)} \left[ \int d\vec{z} \sum_{\lambda} t(\vec{z}, \lambda) \right] = t(\vec{y}, \gamma). \quad (2.6)$$

The equivalent of the change of variable formula is now

$$\frac{\delta\mathcal{F}}{\delta u(\vec{x}, \alpha)} = \int d\vec{y} \sum_{\lambda} \frac{\delta\mathcal{F}}{\delta v(\vec{y}, \lambda)} \frac{\delta v(\vec{y}, \lambda)}{\delta u(\vec{x}, \alpha)}. \quad (2.7)$$

By a generalization of Eq. (2.6), we now have that

$$\begin{aligned} \frac{\delta\Xi}{\delta z^*(\vec{x}, \alpha)} &= \sum_{N=1}^{\infty} \frac{N}{N!} \int d2 \cdots dN \\ &\times \sum_{\lambda_2, \dots, \lambda_N} \prod_{i=2}^N z^*(i, \lambda_i) \prod_{i>j}^N \exp[-\beta V(i, j)], \end{aligned} \quad (2.8)$$

where  $\vec{r}_1 = \vec{x}$  and  $\lambda_1 = \alpha$ . Therefore, comparing with the definition of the  $n$ -density functions, Eq. (2.3), we have that

$$\rho^{(1)}(\vec{x}, \alpha) = \frac{z^*(\vec{x}, \alpha)}{\Xi} \frac{\delta\Xi}{\delta z^*(\vec{x}, \alpha)} = z^*(\vec{x}, \alpha) \frac{\delta \ln \Xi}{\delta z^*(\vec{x}, \alpha)}. \quad (2.9)$$

An immediate generalization yields

$$\begin{aligned} \rho^{(n)}(1, \alpha_1; \dots; n, \alpha_n) &= \frac{1}{\Xi} z^*(1, \alpha_1) \cdots z^*(n, \alpha_n) \\ &\times \frac{\delta^n \Xi}{\delta z^*(1, \alpha_1) \cdots \delta z^*(n, \alpha_n)}. \end{aligned} \quad (2.10)$$

In particular, combining Eqs. (2.9) and (2.10), we have that

$$\begin{aligned} \rho^{(2)}(\vec{x}, \alpha; \vec{y}, \gamma) - \rho^{(1)}(\vec{x}, \alpha) \rho^{(1)}(\vec{y}, \gamma) \\ = z^*(\vec{x}, \alpha) z^*(\vec{y}, \gamma) \frac{\delta \ln \Xi}{\delta z^*(\vec{x}, \alpha) \delta z^*(\vec{y}, \gamma)}. \end{aligned} \quad (2.11)$$

A useful identity is obtained by using Eq. (2.5) in conjunction with Eq. (2.9),

$$\begin{aligned} \frac{\delta \rho^{(1)}(\vec{x}, \alpha)}{\delta \ln[z^*(\vec{y}, \gamma)]} &= z^*(\vec{y}, \gamma) \frac{\delta}{\delta z^*(\vec{y}, \gamma)} \left[ z^*(\vec{x}, \alpha) \frac{\delta \ln \Xi}{\delta z^*(\vec{x}, \alpha)} \right] \\ &= \rho^{(1)}(\vec{x}, \alpha) \delta(\vec{x} - \vec{y}) \delta_{\alpha, \gamma} + \rho^{(1)}(\vec{x}, \alpha) \\ &\quad \times \rho^{(1)}(\vec{y}, \gamma) h^{(2)}(\vec{x}, \alpha; \vec{y}, \gamma), \end{aligned} \quad (2.12)$$

where we have used Eqs. (2.11), (1.8), and (1.9).

By analogy with fluid systems [9], let us now define the spin direct correlation function  $c(\vec{x}, \alpha; \vec{y}, \gamma)$  as

$$c(\vec{x}, \alpha; \vec{y}, \gamma) \equiv \frac{\tilde{\delta} \ln[\rho^{(1)}(\vec{x}, \alpha)/z^*(\vec{x}, \alpha)]}{\delta \rho^{(1)}(\vec{y}, \gamma)}. \quad (2.13)$$

Then, with the identity Eq. (2.5), we have that

$$\frac{\tilde{\delta} \ln[z^*(\vec{x}, \alpha)]}{\delta \rho^{(1)}(\vec{y}, \gamma)} = \frac{1}{\rho^{(1)}(\vec{x}, \alpha)} \delta(\vec{x} - \vec{y}) \delta_{\alpha, \gamma} - c(\vec{x}, \alpha; \vec{y}, \gamma). \quad (2.14)$$

Finally, from the change of variable formula, Eq. (2.7), we have that

$$\begin{aligned} \delta(\vec{x} - \vec{y}) \delta_{\alpha, \gamma} &= \frac{\tilde{\delta} \ln[z^*(\vec{x}, \alpha)]}{\delta \ln[z^*(\vec{y}, \gamma)]} \\ &= \int d\vec{z} \sum_{\lambda} \frac{\tilde{\delta} \ln[z^*(\vec{x}, \alpha)]}{\delta \rho^{(1)}(\vec{z}, \lambda)} \frac{\tilde{\delta} \rho^{(1)}(\vec{z}, \lambda)}{\delta \ln[z^*(\vec{y}, \gamma)]}. \end{aligned} \quad (2.15)$$

Substituting Eqs. (2.12) and (2.13) into Eq. (2.15), we find

$$\begin{aligned} h^{(2)}(\vec{x}, \alpha; \vec{y}, \gamma) &= c(\vec{x}, \alpha; \vec{y}, \gamma) + \int d\vec{z} \sum_{\lambda} \\ &\quad \times \rho^{(1)}(\vec{z}, \lambda) c(\vec{x}, \alpha; \vec{z}, \lambda) h^{(2)}(\vec{z}, \lambda; \vec{y}, \gamma), \end{aligned} \quad (2.16)$$

which is the equivalent, for the Potts fluid, of the classical Ornstein-Zernike relation (see, e.g., Hansen and McDonald [9]).

To find out the implications of this for the percolation system, let us substitute Eq. (2.16) into the definition of the pair connectedness, Eq. (1.9). Then, we have that

$$\begin{aligned} h^{(2)}(\vec{x}, \alpha; \vec{y}, \alpha) - h^{(2)}(\vec{x}, \alpha; \vec{y}, \gamma) &= c(\vec{x}, \alpha; \vec{y}, \alpha) \\ &+ \int d\vec{z} \rho^{(1)}(\vec{z}, \alpha) c(\vec{x}, \alpha; \vec{z}, \alpha) h^{(2)}(\vec{z}, \alpha; \vec{y}, \alpha) \\ &+ \int d\vec{z} \sum_{\lambda \neq \alpha} \rho^{(1)}(\vec{z}, \lambda) c(\vec{x}, \alpha; \vec{z}, \lambda) h^{(2)}(\vec{z}, \lambda; \vec{y}, \alpha) \\ &- c(\vec{x}, \alpha; \vec{y}, \gamma) - \int d\vec{z} \rho^{(1)}(\vec{z}, \alpha) c(\vec{x}, \alpha; \vec{z}, \alpha) \\ &\times h^{(2)}(\vec{z}, \alpha; \vec{y}, \gamma) - \int d\vec{z} \rho^{(1)}(\vec{z}, \gamma) c(\vec{x}, \alpha; \vec{z}, \gamma) \\ &\times h^{(2)}(\vec{z}, \gamma; \vec{y}, \gamma) - \int d\vec{z} \sum_{\substack{\lambda \neq \alpha \\ \lambda \neq \gamma}} \rho^{(1)}(\vec{z}, \lambda) c(\vec{x}, \alpha; \vec{z}, \lambda) \\ &\times h^{(2)}(\vec{z}, \lambda; \vec{y}, \gamma). \end{aligned} \quad (2.17)$$

We use now the fact that for  $\rho < \rho_c$  the symmetry of the system is unbroken and therefore

$$\rho^{(1)}(\vec{z}, \lambda) = \frac{1}{s} \rho(\vec{z}), \quad (2.18)$$

where  $\rho(\vec{z})$  is the local density at  $\vec{z}$ . For the same reason, we also have that

$$\begin{aligned} c(\vec{x}, \alpha; \vec{y}, \alpha) &= c(\vec{x}, \gamma; \vec{y}, \gamma), \\ h^{(2)}(\vec{x}, \alpha; \vec{y}, \alpha) &= h^{(2)}(\vec{x}, \gamma; \vec{y}, \gamma), \end{aligned} \quad (2.19)$$

$$h^{(2)}(\vec{x}, \alpha; \vec{y}, \gamma) = h^{(2)}(\vec{x}, \alpha; \vec{y}, \lambda),$$

for any spins  $\gamma, \lambda \neq \alpha$ , and other similar relations. Then we can rewrite Eq. (2.17) as

$$\begin{aligned} h^{(2)}(\vec{x}, \alpha; \vec{y}, \alpha) - h^{(2)}(\vec{x}, \alpha; \vec{y}, \gamma) &= c(\vec{x}, \alpha; \vec{y}, \alpha) - c(\vec{x}, \alpha; \vec{y}, \gamma) \\ &+ \frac{1}{s} \int d\vec{z} \rho(\vec{z}) c(\vec{x}, \alpha; \vec{z}, \alpha) h^{(2)}(\vec{z}, \alpha; \vec{y}, \alpha) \\ &+ \frac{s-1}{s} \int d\vec{z} \rho(\vec{z}) c(\vec{x}, \alpha; \vec{z}, \gamma) h^{(2)}(\vec{z}, \gamma; \vec{y}, \gamma) \\ &- \frac{1}{s} \int d\vec{z} \rho(\vec{z}) c(\vec{x}, \alpha; \vec{z}, \alpha) h^{(2)}(\vec{z}, \alpha; \vec{y}, \gamma) \\ &- \frac{1}{s} \int d\vec{z} \rho(\vec{z}) c(\vec{x}, \alpha; \vec{z}, \gamma) h^{(2)}(\vec{z}, \alpha; \vec{y}, \alpha) \\ &- \frac{s-2}{s} \int d\vec{z} \rho(\vec{z}) c(\vec{x}, \alpha; \vec{z}, \gamma) h^{(2)}(\vec{z}, \gamma; \vec{y}, \gamma). \end{aligned} \quad (2.20)$$

Finally, we can take the limit  $s \rightarrow 1$ . Equation (2.20) then becomes

$$\begin{aligned} \lim_{s \rightarrow 1} [h^{(2)}(\vec{x}, \alpha; \vec{y}, \alpha) - h^{(2)}(\vec{x}, \alpha; \vec{y}, \gamma)] &= \lim_{s \rightarrow 1} \left\{ [c(\vec{x}, \alpha; \vec{y}, \alpha) - c(\vec{x}, \alpha; \vec{y}, \gamma)] \right. \\ &\quad + \int d\vec{z} \rho(\vec{z}) [c(\vec{x}, \alpha; \vec{z}, \alpha) - c(\vec{x}, \alpha; \vec{z}, \gamma)] \\ &\quad \times [h^{(2)}(\vec{z}, \alpha; \vec{y}, \alpha) - h^{(2)}(\vec{z}, \alpha; \vec{y}, \gamma)] \left. \right\}. \end{aligned} \quad (2.21)$$

We can now define a percolation direct connectedness function  $c^\dagger(\vec{x}, \vec{y})$  as

$$c^\dagger(\vec{x}, \vec{y}) = \lim_{s \rightarrow 1} [c(\vec{x}, \alpha; \vec{y}, \alpha) - c(\vec{x}, \alpha; \vec{y}, \gamma)]. \quad (2.22)$$

Equation (2.21) then becomes, with the help of the definition of the pair connectedness, Eq. (1.16),

$$g^\dagger(\vec{x}, \vec{y}) = c^\dagger(\vec{x}, \vec{y}) + \int d\vec{z} \rho(\vec{z}) c^\dagger(\vec{x}, \vec{z}) g^\dagger(\vec{z}, \vec{y}), \quad (2.23)$$

which is the percolation analog of the Ornstein-Zernike relation. This relation will prove useful in the next section.



$$\ln[\rho^{(1)}(\vec{x}, \alpha)/z^*(\vec{x}, \alpha)] = \{\text{all simple diagrams consisting of one white 1 circle labeled } (\vec{x}, \alpha), \\ \text{one or more black } \rho^{(1)} \text{ circles and } \phi \text{ bonds, such that they are free of connecting circles}\}. \quad (3.10)$$

A connecting circle is a circle the removal of which (along with the bonds which emerge from it) causes the diagram to become disconnected.

From Eq. (2.13) and the lemma (3.8), we immediately obtain that

$$c(\vec{x}, \alpha; \vec{y}, \gamma) = \{\text{all simple diagrams that consist of two white 1 circles labeled } (\vec{x}, \alpha), \text{ and } (\vec{y}, \gamma), \\ \text{black } \rho^{(1)} \text{ circles and } \phi \text{ bonds, and are free of connecting circles}\} \\ = \text{---} + \text{---} + \text{---} + \text{---} + \dots \quad (3.11)$$

In all these diagrams, one of the white circles is labeled  $(\vec{x}, \alpha)$  and the other is labeled  $(\vec{y}, \gamma)$ .

The Ornstein-Zernike relation, Eq. (2.16), now determines  $h^{(2)}$ . For vanishing magnetic field  $h=0$ , we have significant simplifications, since  $\rho^{(1)}(\vec{z}, \lambda) = (1/s)\rho$ , where  $\rho = \langle N \rangle / V$  is the usual density. Furthermore,  $h^{(2)}(\vec{x}, \alpha; \vec{y}, \gamma)$  and  $c(\vec{x}, \alpha; \vec{y}, \gamma)$  now depend on  $\vec{x} - \vec{y}$  provided  $v(\vec{x}, \vec{y}) = v(\vec{x} - \vec{y})$  and  $p(\vec{x}, \vec{y}) = p(\vec{x} - \vec{y})$ , which we always assume. In this case, the Ornstein-Zernike relation is very simple in Fourier space, i.e.,

$$\hat{h}^{(2)}(\vec{k}, \alpha, \gamma) = \frac{\hat{c}(\vec{k}, \alpha, \gamma)}{1 - (\rho/s)\hat{c}(\vec{k}, \alpha, \gamma)}, \quad (3.12)$$

where

$$\hat{h}^{(2)}(\vec{k}, \alpha, \gamma) = \int d\vec{x} e^{-i\vec{k}(\vec{x}-\vec{y})} h^{(2)}(\vec{x}, \alpha; \vec{y}, \gamma), \\ \hat{c}(\vec{k}, \alpha, \gamma) = \int d\vec{x} e^{-i\vec{k}(\vec{x}-\vec{y})} c(\vec{x}, \alpha; \vec{y}, \gamma). \quad (3.13)$$

Going now to the percolation picture, we notice that Eq. (1.15) for  $S$  can be rewritten

$$S = 1 + \rho \hat{g}^\dagger(0). \quad (3.14)$$

From the definition of  $\hat{g}^\dagger$ , Eq. (1.16), and from Eqs. (2.23), (2.22), and (3.12), we have now

$$S = \frac{1}{1 - \rho \hat{c}^\dagger(0)} = \frac{1}{1 - \rho \lim_{\substack{s \rightarrow 1 \\ h \rightarrow 0}} [\hat{c}(0, \alpha, \alpha) - \hat{c}(0, \alpha, \gamma)]}. \quad (3.15)$$

This equation, together with the expansion of  $c(\vec{x}, \alpha; \vec{y}, \gamma)$ , Eq. (3.11), defines an expansion of  $S$  in powers of the density. The critical density  $\rho_c$  is the radius of convergence of this series, which we can find by using standard methods of convergence analysis (see, e.g., Refs. [19,20]).

#### IV. EQUIVALENCE WITH CONIGLIO-DeANGELIS-FORLANI EXPANSION

In 1977, Coniglio, DeAngelis, and Forlani (CDF) [8] obtained a density expansion for  $c^\dagger(\vec{x}, \vec{y})$  from a completely different point of view. We discuss now the connection of the present work to the CDF expansion.

Coniglio, DeAngelis, and Forlani start by considering a classical fluid (no spins), where the interparticle interaction is  $v(i, j)$ . For this fluid, the classical Ornstein-Zernike direct correlation function  $c_f(\vec{x}, \vec{y})$  has a density expansion given by Eq. (3.11), except that the white 1 circles are labeled just  $\vec{x}$  and  $\vec{y}$  and the bonds represent the Mayer  $f$  function defined as  $f(i, j) \equiv \exp[-\beta v(i, j)] - 1$ , in the same notation used here in Eq. (3.3). Coniglio, DeAngelis, and Forlani then assume that the Mayer  $f$  function can be decomposed into a sum  $f(i, j) = f^\dagger(i, j) + f^*(i, j)$  where  $f^\dagger$  is related to the particles being connected and  $f^*$  to their being unconnected. The specific definitions of  $f^\dagger$  and  $f^*$  used by Coniglio, DeAngelis, and Forlani are relevant only to physical clustering in a gas, but the assumption of the decomposition of  $f(i, j)$  was extended by analogy to other systems by several workers [3,10,11]. If we take  $f^*$  as formally defined here in Eq. (3.3), which is natural since this function is directly related to the probability of the two particles being unconnected, we find that

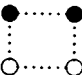
$$f^\dagger(i, j) \equiv f(i, j) - f^*(i, j) = p(i, j) \exp[-\beta v(i, j)]. \quad (4.1)$$

This result is satisfying since  $f^\dagger$  turns out to be directly proportional to the probability of the two particles being connected.

Coniglio, DeAngelis, and Forlani then replace  $f$  in the diagrammatic expansion of  $c_f(\vec{x}, \vec{y})$ , with the sum  $f^\dagger + f^*$ , and consider all the decomposed diagrams thus obtained, in which every bond is either an  $f^\dagger$  or an  $f^*$  function. The sum of all the diagrams which contain at least one continuous path of  $f^\dagger$  functions between the white 1 circles, they consider to be  $c^\dagger(\vec{x}, \vec{y})$ , while the remainder is called  $c^*(\vec{x}, \vec{y})$ , so that  $c_f(\vec{x}, \vec{y}) = c^\dagger(\vec{x}, \vec{y}) + c^*(\vec{x}, \vec{y})$ .

It is hardly obvious now that this algorithm agrees with the expansion obtained here. Indeed, the function  $f^\dagger$  never appears in the present expansion. Nonetheless, the two formulations are equivalent.

The principle of equivalence holds diagram by diagram. Therefore, for simplicity a specific example, e.g.,

the diagram  in this diagram, every dotted line denotes a function  $f(i, j)$ . Then, if we consider all the diagrams obtained by replacing every  $f$  bond by either an  $f^*$  bond or an  $f^\dagger$  bond in all possible ways, and keep only those diagrams which contain a continuous  $f^\dagger$  path between the two white circles, we obtain

$$\text{CDF} \left[ \begin{array}{cc} \bullet & \bullet \\ \vdots & \vdots \\ \circ & \circ \end{array} \right] = \begin{array}{cc} \bullet & \bullet \\ \text{---} & \text{---} \\ \circ & \circ \end{array} + \begin{array}{cc} \bullet & \bullet \\ \vdots & \vdots \\ \circ & \text{---} \end{array}, \quad (4.2)$$

where a double line denotes a function  $f^\dagger(i, j)$ , and  $\text{CDF}[\text{diagram}]$  on the left hand side means the result of the CDF algorithm when applied to the given diagram. The dotted lines on the right hand side ( $f$  bonds) arise because once a continuous  $f^\dagger$  path exists, all the diagrams obtained from further replacements of  $f$  bonds by  $f^\dagger$  bonds and  $f^*$  bonds must be counted. This sum can be expressed more compactly by keeping the original  $f$  bonds.

We now wish to prove the equivalence of this scheme to the one we have developed here, i.e.,

$$\text{CDF} \left[ \begin{array}{cc} \bullet & \bullet \\ \vdots & \vdots \\ \circ & \circ \end{array} \right] = \lim_{s \rightarrow 1} \left[ \begin{array}{cc} \bullet & \bullet \\ \text{---} & \text{---} \\ \alpha & \alpha \end{array} - \begin{array}{cc} \bullet & \bullet \\ \text{---} & \text{---} \\ \alpha & \eta \end{array} \right], \quad (4.3)$$

where on the right hand side, every diagram is of the spin type, and every full line represents a function  $\phi(i, j)$ . To simplify still further, let us ignore the integration over the coordinates of the black circles (but *not* the summation over spins in the spin diagrams). The integrals can then be added at the end of the proof. E.g., in this section we shall assume that


$$\begin{array}{cc} \bullet & \bullet \\ \vdots & \vdots \\ \circ & \circ \end{array} = \begin{array}{cc} 3 & 4 \\ \bullet & \bullet \\ \vdots & \vdots \\ 1 & 2 \\ \circ & \circ \end{array} = f(1, 3)f(3, 4)f(4, 2)f(1, 2), \quad (4.4)$$

and

$$\begin{array}{cc} 3 & 4 \\ \bullet & \bullet \\ \text{---} & \text{---} \\ 1, \alpha & 2, \eta \\ \circ & \circ \end{array} = \sum_{\lambda_3, \lambda_4} \phi(1, 3)\phi(3, 4)\phi(4, 2)\phi(1, 2), \quad (4.5)$$

where the labels 1, 2, 3, 4 denote the spatial coordinates of the vertices. Note that in the last diagram,  $\lambda_1 = \alpha$ ,  $\lambda_2 = \eta$  are fixed, but we sum over the spins  $\lambda_3$  and  $\lambda_4$ .

With this convention, we are ready to prove the equivalence of the two formulations. To do this, let us define a new "percolation" problem on the four-vertex

graph  In this new problem, every bond can be

either "open" (in which case its two ends are said to be connected) or closed (in which case the ends are disconnected). Let us further assume that the bond connecting the vertices  $i$  and  $j$  is open with a probability  $f^\dagger(i, j)$  and closed with a probability  $f^*(i, j)$ . Formally these are not true probabilities since their sum is not normalized to 1, but this is of no importance. One can always normalize the probabilities

by dividing by the proper product of  $f$  functions. With this convention, every diagram obtained from the CDF algorithm now represents the (*unnormalized*) probability of a specific configuration of open and closed bonds on the four-vertex graph. E.g., consider

$$\begin{array}{cc} \bullet & \bullet \\ \text{---} & \text{---} \\ \circ & \circ \end{array} = f^\dagger(1, 3)f^\dagger(3, 4)f^\dagger(4, 2)f^*(1, 2), \quad (4.6)$$

where a line of \* represents a function  $f^*$ . The same diagram can also be thought of as a configuration of open and closed bonds on the four-vertex graph, by letting a double line represent an open bond and a \* line a closed bond. This geometrical configuration occurs with a probability  $f^\dagger(1, 3)f^\dagger(3, 4)f^\dagger(4, 2)f^*(1, 2)$ , which is just the value of the equivalent diagram, Eq. (4.6). Every diagram therefore functions in a double capacity. On the one hand, it represents an

actual configuration of open and closed bonds on some graph. On the other hand, it represents some functional value. This functional value is just the (unnormalized) probability of the bond configuration represented by the same graph.

Now, two vertices which are connected by a path of open bonds can be said to belong to the same cluster. In particular, the (unnormalized) probability that the two white circles belong to the same cluster, denoted  $P_{cl}(1,2)$ , is the sum of all the diagrams in which a continuous path of open bonds exists between these circles. This, however, is exactly the class of diagrams selected by the CDF algorithm. Hence,

$$P_{cl}(1,2) = \text{CDF} \left[ \begin{array}{c} \bullet \cdots \bullet \\ \vdots \quad \vdots \\ \circ \cdots \circ \end{array} \right]. \quad (4.7)$$

Therefore what we now need to prove is that

$$P_{cl}(1,2) = \lim_{s \rightarrow 1} \left[ \begin{array}{c} \bullet \cdots \bullet \\ \vdots \quad \vdots \\ \circ \cdots \circ \\ \alpha \quad \alpha \end{array} - \begin{array}{c} \bullet \cdots \bullet \\ \vdots \quad \vdots \\ \circ \cdots \circ \\ \alpha \quad \eta \end{array} \right]. \quad (4.8)$$

To probe this we show, by paralleling the derivation given in I, that there exists a mapping of the new bond-percolation problem onto an  $s$ -spin model. Then  $P_{cl}(1,2)$  (which plays here the part of the pair connectedness) is equal to the difference of two spin diagrams. The formal proof of this claim is given in the Appendix. It is easily seen to hold for every diagram in the CDF expansion, and shows therefore that this expansion is indeed equivalent to the one derived here in the context of the Potts fluid.

## V. APPLICATION TO EXTENDED HYPERCUBES

Let us see now how the expansion obtained in Sec. III can be applied to finding the critical density  $\rho_c$ . The system we consider consists of  $D$ -dimensional hypercubes which have an impenetrable (hard) core of side  $a$ , surrounded with a hypercubic permeable shell of side  $d > a$ , so that two particles are bound if their shells overlap. In other words, if  $\vec{r}_i = (x_i^1, \dots, x_i^D)$  and  $\vec{r}_j = (x_j^1, \dots, x_j^D)$  are the positions of two particles, then

$$v(i,j) = \begin{cases} \infty & \text{if for all } 1 \leq k \leq D, |x_i^k - x_j^k| < a \\ 0 & \text{otherwise} \end{cases} \quad (5.1)$$

$$p(i,j) = \begin{cases} 1 & \text{if for all } 1 \leq k \leq D, |x_i^k - x_j^k| < d \\ 0 & \text{otherwise.} \end{cases} \quad (5.2)$$

Hence, from Eq. (3.3),

$$f(\vec{r}_i, \vec{r}_j) = \begin{cases} -1 & \text{if for all } 1 \leq k \leq D, |x_i^k - x_j^k| < a \\ 0 & \text{otherwise.} \end{cases} \quad (5.3)$$

$$f^*(\vec{r}_i, \vec{r}_j) = \begin{cases} -1 & \text{if for all } 1 \leq k \leq D, |x_i^k - x_j^k| < d \\ 0 & \text{otherwise.} \end{cases} \quad (5.4)$$

We choose this rather unrealistic system because for any dimension  $D$  the required calculations always turn out to be much simpler for cubes than for the more realistic spheres. Since the aim at present is to prove the usefulness of the method rather than investigate a specific system, one should not be overly troubled by this choice. Let us note, however, that the spherical version of this model has been used to model microemulsions [3], so that it is at least mildly relevant to some real systems. It is also the simplest model which contains interactions, and therefore a good testing case.

Let us now define two functions of a single variable,

$$F_1(x) = \begin{cases} 1 & \text{if } |x| < a \\ 0 & \text{if } |x| > a. \end{cases} \quad (5.5)$$

$$F_2(x) = \begin{cases} 1 & \text{if } |x| < d \\ 0 & \text{if } |x| > d. \end{cases} \quad (5.6)$$

Equations (5.4) can now be rewritten as

$$f(x^1, \dots, x^D) = - \prod_{i=1}^D F_1(x^i). \quad (5.7)$$

$$f^*(x^1, \dots, x^D) = - \prod_{i=1}^D F_2(x^i). \quad (5.8)$$

We shall now calculate  $c^\dagger$  up to the second order in  $\rho$  (i.e., up to square diagrams). The zeroth order is

$$\lim_{s \rightarrow 1} \left[ \begin{array}{c} \circ \cdots \circ \\ \alpha \quad \alpha \end{array} - \begin{array}{c} \circ \cdots \circ \\ \alpha \quad \gamma \end{array} \right] = \int d\vec{z} [f(\vec{z}) - f^*(\vec{z})] = (2d)^D (1 - \eta^D), \quad (5.9)$$

where we have defined the aspect ratio  $\eta$  as

$$\eta \equiv \frac{a}{d}. \quad (5.10)$$

For the first order (triangular diagrams), we need, e.g., the integral

$$\Omega(\vec{y}) \equiv \int d\vec{x} f(\vec{x}) f(\vec{x} - \vec{y}) = \prod_{i=1}^D \left\{ \int dx^i F_1(x^i) F_1(x^i - y^i) \right\}. \quad (5.11)$$

It is precisely the factorization of this and similar integrals into a product of identical one-dimensional integrals that is the main simplification afforded by the use of a cubic geom-



TABLE I. The integrals contributed by triangular diagrams. The first column is the notation and the last is the value. This value is the  $D$ th power of the one-dimensional integral whose integrand occupies the second column. The variables  $x$  and  $y$  are integrated upon.

$I_1$	$F_1(x)F_1(x-y)F_1(y)$	$(3a^2)^D$
$I_2$	$F_2(x)F_2(x-y)F_1(y)$	$(4da-a^2)^D$
$I_3$	$F_2(x)F_2(x-y)F_2(y)$	$(3d^2)^D$

etry. As a beneficial side effect, it allows us to check the influence of system dimensionality on the critical density.

$\Omega(\vec{y})$  is very simple to evaluate when we realize that  $\int dx F_1(x)F_1(x-y)$  is merely the overlap of two segments of length  $2a$ , one of which is centered at the origin, the other centered at the position  $y$ . By direct inspection, we have therefore that

$$\int dx F_1(x)F_1(x-y) = \begin{cases} 2a-|y| & \text{if } |y| < 2a \\ 0 & \text{if } |y| > 2a, \end{cases} \quad (5.12)$$

$$\int dx F_2(x)F_2(x-y) = \begin{cases} 2d-|y| & \text{if } |y| < 2d \\ 0 & \text{if } |y| > 2d, \end{cases} \quad (5.13)$$

$$\int dx F_1(x)F_2(x-y) = \begin{cases} 2a & \text{if } |y| < d-a \\ d+a-|y| & \text{if } d-a < |y| < d+a \\ 0 & \text{if } |y| > d+a. \end{cases} \quad (5.14)$$

Let us consider a typical contribution from the triangular diagrams, e.g., the integral  $\int dx dy F_2(x)F_2(x-y)F_1(y)$ . In this integral, we interpret the term  $F_1(y)$  as merely specifying the limits of integration, i.e., determining that  $|y| < a$ . Since  $d > a$ , we have from Eq. (5.13) that

$$\begin{aligned} & \int dx dy F_2(x)F_2(x-y)F_1(y) \\ &= \int_{-a}^a dy \left[ \int dx F_2(x)F_2(x-y) \right] = 4da - a^2. \end{aligned} \quad (5.15)$$

All the required one-dimensional integrals can now be calculated along the same lines. In fact, Eqs. (5.12)–(5.14) suffice to calculate all the triangular and square diagrams, except for the last fully connected square diagram which is a product of six  $F$  functions. For this diagram the previous arguments have to be generalized but it can be done easily along the lines already presented.

All the integrals we need are presented in Tables I–IV. The first column in each table contains the notation of the integral, and the third column its value. All these integrals are  $D$ th powers of some one-dimensional integrals [see, e.g., Eq. (5.11)]. The corresponding one-dimensional integrals appear in the second column.

We now have, after some straightforward calculations, that the contribution of the triangular diagrams, denoted  $(2d)^{2D}k_2$ , is, in the notation of Tables I–IV,

$$(2d)^{2D}k_2 = I_1 - 2I_2 + I_3. \quad (5.16)$$

TABLE II. The integrals contributed by square diagrams with four lines. The first column is the notation and the last is the value. This value is the  $D$ th power of the one-dimensional integral whose integrand occupies the second column. The variables  $x$ ,  $y$ , and  $z$  are integrated upon.

$J_1$	$F_1(x)F_1(x-y)F_1(z)F_1(z-y)$	$(\frac{16}{3}a^3)^D$
$J_2$	$F_1(x)F_1(x-y)F_2(z)F_2(z-y)$	$(8da^2 - \frac{1}{3}a^3)^D$
$J_3$	$F_1(x)F_2(x-y)F_2(z)F_2(z-y)$	$(6d^2a - \frac{2}{3}a^3)^D$
$J_4$	$F_2(x)F_2(x-y)F_2(z)F_2(z-y)$	$(\frac{16}{3}d^3)^D$

Similarly, the contribution from the square diagrams is denoted  $(2d)^{3D}k_3$ , and in the notation of Tables I–IV is equal to

$$\begin{aligned} (2d)^{3D}k_3 = & \frac{3}{2}J_1 - 5J_2 + 5J_3 - \frac{3}{2}J_4 - 3K_1 + 3K_2 - \frac{1}{2}K_3 + 7K_4 \\ & - 10K_5 + \frac{7}{2}K_6 + \frac{1}{2}L_1 - L_2 - L_3 + \frac{5}{2}L_4 - L_5. \end{aligned} \quad (5.17)$$

Substituting these results into Eq. (3.15) yields, for the mean cluster size,

$$\begin{aligned} S &= \frac{1}{1 - \rho(2d)^D(1 - \eta^D) - \rho^2(2d)^{2D}k_2 - \rho^3(2d)^{3D}k_3 + O(\rho^4)}. \end{aligned} \quad (5.18)$$

The critical density is commonly measured in dimensionless units. Let us define

$$B = (2d)^D \rho, \quad (5.19)$$

which is chosen to reduce to the total excluded volume when  $a \rightarrow 0$  [7]. As mentioned in the Introduction, this reduces the dependence of the density on the details of the system and facilitates the presentation of the results. Finally, using standard methods [21], we find the series expansion for the mean cluster size to be

$$S = 1 + S_1 B + S_2 B^2 + S_3 B^3 + O(B^4), \quad (5.20)$$

with

$$S_1 = 1 - \eta^D,$$

$$S_2 = k_2 + S_1^2,$$

$$S_3 = k_3 + 2S_1 k_2 + S_1^3. \quad (5.21)$$

## VI. RESULTS FOR HYPERCUBES

To find the critical density, we need some extrapolation method which will yield the point of divergence of the series (5.20). Unfortunately, we know very few terms in this series. The results can be improved, however, by using additional information. In particular,  $S$  diverges as  $S \sim (B_c - B)^{-\gamma}$ , and  $\gamma$  appears to be universal, i.e., independent of the interaction, and furthermore, equal to the well known value it takes in lattice percolation. *Biased methods* use the known value of  $\gamma$  to calculate  $B_c$ . There are several methods available, but for the present use, the best seems to be the one developed by

TABLE III. The integrals contributed by square diagrams with five lines. The first column is the notation and the last is the value. This value is the  $D$ th power of the one-dimensional integral whose integrand occupies the second column. The variables  $x$ ,  $y$ , and  $z$  are integrated upon.

$K_1$	$F_1(y)F_1(x)F_1(x-y)F_1(z)F_1(z-y)$	$(\frac{14}{3}a^3)^D$
$K_2$	$F_1(y)F_1(x)F_1(x-y)F_2(z)F_2(z-y)$	$(6da^2 - \frac{4}{3}a^3)^D$
$K_3$	$F_1(y)F_2(x)F_2(x-y)F_2(z)F_2(z-y)$	$(8d^2a - 4da^2 + \frac{2}{3}a^3)^3$
$K_4$	$F_2(y)F_1(x)F_2(x-y)F_1(z)F_2(z-y)$	$(8da^2 - \frac{10}{3}a^3)^D$
$K_5$	$F_2(y)F_1(x)F_2(x-y)F_2(z)F_2(z-y)$	$(6d^2a - da^2 - \frac{1}{3}a^3)^D$
$K_6$	$F_2(y)F_2(x)F_2(x-y)F_2(z)F_2(z-y)$	$(\frac{14}{3}d^3)^D$

Arteca, Fernandez, and Castro (AFC) [22]. The biased version of this method relies on the fact that the function  $(B_c - B)^\gamma S(B)$  is analytical around  $B_c$ . Therefore we define a function of two variables,

$$g(u, B) = \left(1 - \frac{B}{u}\right)^\gamma S(B), \quad (6.1)$$

where we have assumed a known value for  $\gamma$ . Given an expansion  $S = \sum S_n B^n$ , we can expand  $g(u, B)$  in powers of  $B$ , with the result

$$g(u, B) = \sum_{n=0}^{\infty} g_n(u) B^n, \quad (6.2)$$

where

$$g_n(u) = \sum_{k=0}^n \binom{\gamma}{k} (-u)^{-k} S_{n-k}. \quad (6.3)$$

Since  $g(u, B)$  is analytical at  $u = B_c$ , the idea is now to look for values of  $u$  which maximize the convergence of the series  $\{g_n(u)\}_{n=1}^{\infty}$  as  $n \rightarrow \infty$ . The AFC proposal is to generate a series  $\{u_n\}_{n=1}^{\infty}$  of solutions of the equation

$$g_n(u_n) = 0. \quad (6.4)$$

Then we expect that

$$\lim_{n \rightarrow \infty} u_n = B_c. \quad (6.5)$$

In the case of the series (5.20), we know the terms only up to  $n=3$ , which is too little to extrapolate a reliable limit to the series  $\{u_n\}_{n=1}^{\infty}$ . Therefore we take simply the last term of the series,  $u_3$ , as our estimate of  $B_c$ .

In Figs. 1–4, we compare this theoretical estimate to results of computer simulations for dimensions 2, 3, 4, and 5, as a function of the aspect ratio  $\eta$ . The simulations were

performed with an efficient algorithm we introduced recently for investigating continuum percolation with interactions [23]. Unlike the usual Metropolis algorithm, this method increases serially the density in the system until percolation is achieved. The effect of the interactions is included through a rejection criterion which produces an effective statistical weight for the configurations. The final (percolating) configuration contained close to 30 000 particles in two and three dimensions and around 10 000 in the higher dimensions. The results are averages over ten independent runs and the numerical error is estimated to range from 5% to 10%.

Let us first consider the well reproduced qualitative behavior of  $B_c(\eta)$ . The main features can be understood from simple arguments. As pointed out by Bug *et al.* [3], the minimum of  $B_c(\eta)$  results from the competition between two processes. As the diameter of the hard core increases, it becomes harder to bring particles close enough to each other for them to bind. This effect clearly dominates at high  $\eta$ . At low  $\eta$ , on the other hand, the hard core is much too small relative to the soft shell to prevent binding significantly, but it increases the average distance between bound particles. As a result the clusters are “longer,” and therefore percolate “sooner,” hence  $B_c$  is lower.

The dependence on  $D$  is understandable in terms of the ratio of the permeable shell volume to the hard core volume. Clearly, this ratio increases with the dimensionality. Therefore, at any given  $\eta$ , the influence of the hard core diminishes as  $D$  increases. As a result, the graph of  $B_c(\eta)$  looks flatter, while the influence of the final singularity at  $\eta=1$  (at which there is no possibility of binding anymore and therefore no percolating phase), is limited to regions of higher  $\eta$ . This also influences the feasibility of the simulations. Clearly, the larger the hard core, i.e., the greater  $\eta$ , the harder it is to simulate the system. Hence, e.g., in two dimensions, we have no results beyond  $\eta=0.8$  due to this difficulty. As  $D$  increases, however, higher  $\eta$  become more accessible. Unfortunately, it is generally harder to simulate high-dimensional systems, which is why we stopped at  $D=5$ . The

TABLE IV. The integrals contributed by square diagrams with six lines. The first column is the notation and the last is the value. This value is the  $D$ th power of the one-dimensional integral whose integrand occupies the second column. The variables  $x$ ,  $y$ , and  $z$  are integrated upon.

$L_1$	$F_1(x)F_1(y)F_1(z)F_1(x-y)F_1(x-z)F_1(z-y)$	$(4a^3)^D$
$L_2$	$F_2(x)F_2(y)F_2(z)F_1(x-y)F_1(x-z)F_1(z-y)$	$(6da^2 - 2a^3)^D$
$L_3$	$F_1(x)F_2(y)F_2(z)F_2(x-y)F_2(x-z)F_1(z-y)$	$(8da^2 - 4a^3)^D$
$L_4$	$F_2(x)F_2(y)F_2(z)F_2(x-y)F_2(x-z)F_1(z-y)$	$(6d^2a - 2da^2)^D$
$L_5$	$F_2(x)F_2(y)F_2(z)F_2(x-y)F_2(x-z)F_2(z-y)$	$(4d^3)^D$

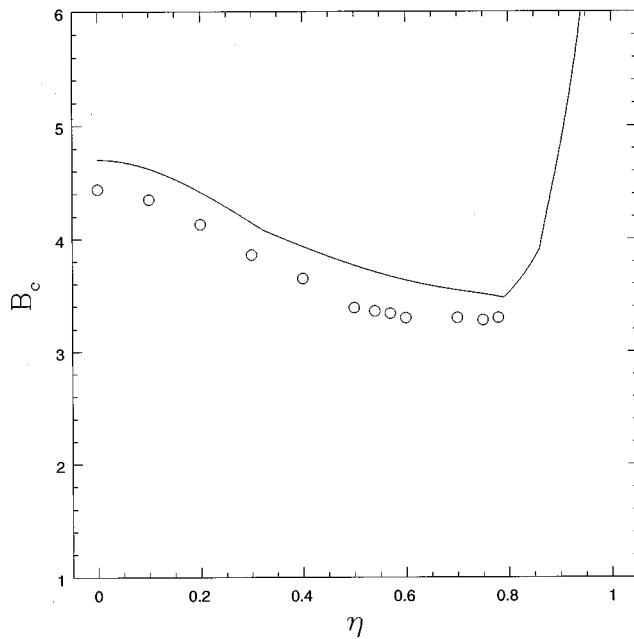


FIG. 1. The percolation threshold  $B_c$  as a function of the aspect ratio for hard core squares with a soft shell, in dimension 2. The line represents the theoretical calculation, obtained from the AFC algorithm, biased with a value of  $\gamma = \frac{43}{18}$  [24]. The circles are the results of computer simulations.

trends are obvious, however, and there should be nothing exceptional for  $D > 5$ . Even though we did not perform simulations for dimensions higher than 5, we could easily calculate the theoretical prediction for  $D=6$  (Fig. 5) and  $D=7$  (Fig. 6) which show the expected continuation of the previ-

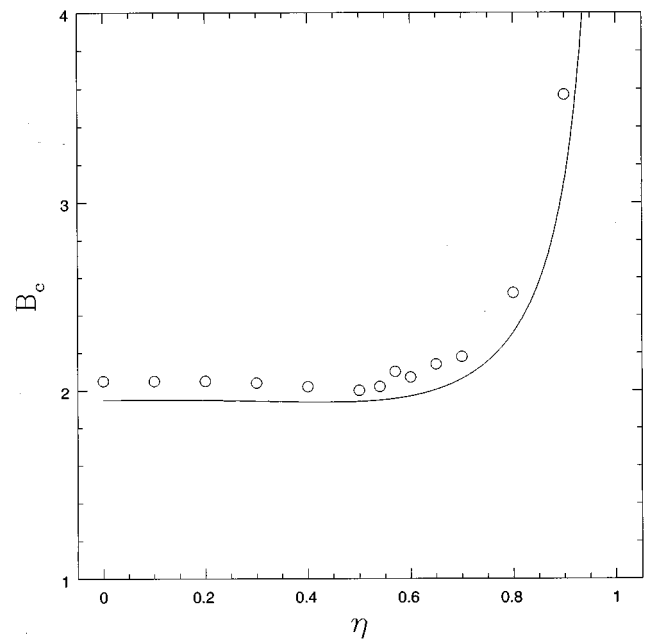


FIG. 3. The percolation threshold  $B_c$  as a function of the aspect ratio for hard core hypercubes with a soft shell in dimension 4. The line represents the theoretical calculation, obtained from the AFC algorithm, biased with a value of  $\gamma = 1.44$  [24]. The circles are the results of computer simulations.

ously mentioned trends. Interested researchers might want to perform simulations to compare with these results.

Turning now to the detailed comparison between theory and simulations, we see that the results are quantitatively close to each other. Even in the worse case, in two dimen-

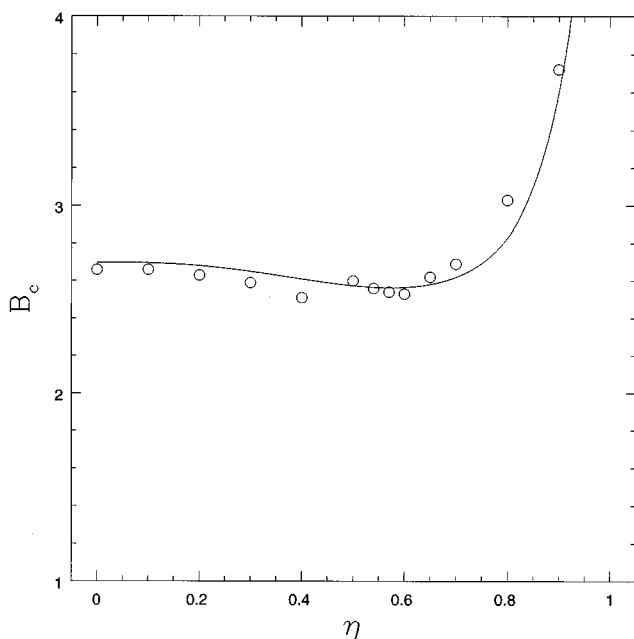


FIG. 2. The percolation threshold  $B_c$  as a function of the aspect ratio for hard core cubes with a soft shell, in dimension 3. The line represents the theoretical calculation, obtained from the AFC algorithm, biased with a value of  $\gamma = 1.74$  [25]. The circles are the results of computer simulations.

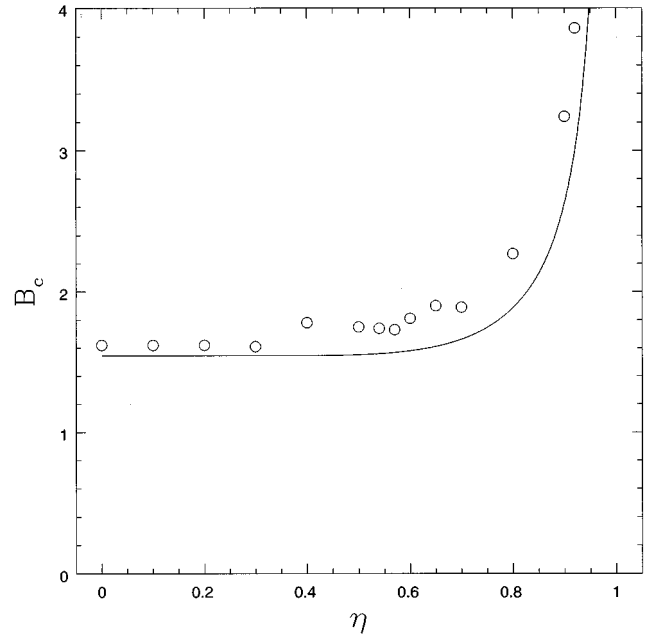


FIG. 4. The percolation threshold  $B_c$  as a function of the aspect ratio for hard core hypercubes with a soft shell in dimension 5. The line represents the theoretical calculation, obtained from the AFC algorithm, biased with a value of  $\gamma = 1.2$  [24]. The circles are the results of computer simulations.

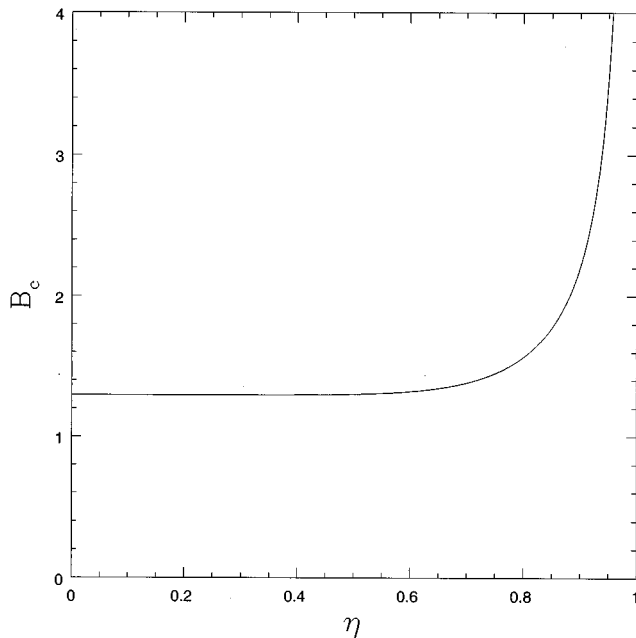


FIG. 5. The percolation threshold  $B_c$  as a function of the aspect ratio for hard core hypercubes with a soft shell in dimension 6. The line represents the theoretical calculation, obtained from the AFC algorithm, biased with a value of  $\gamma=1.0$  [24].

sions (Fig. 1), the difference between theory and simulations is at most 11% (at  $\eta=0.5$ ). The position of the minimum, theoretically predicted to be  $\eta=0.79$ , also agrees well with the simulations. We would like to note as an aside that very recently Okazaki *et al.* [6] have performed new simulations of two-dimensional continuum percolation, and have obtained a value  $\gamma=1.94$  instead of the higher  $\frac{43}{18}$  obtained in

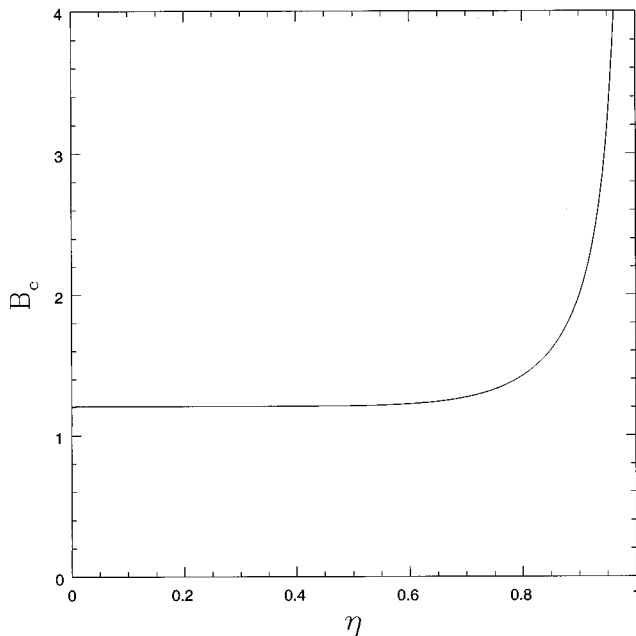


FIG. 6. The percolation threshold  $B_c$  as a function of the aspect ratio for hard core hypercubes with a soft shell in dimension 7. The line represents the theoretical calculation, obtained from the AFC algorithm, biased with a value of  $\gamma=1.0$  [24].

lattice percolation [24]. Use of this value to bias the theory would yield a sensibly better fit to the simulations, with deviations under 5%. Since, however, the results of Okazaki *et al.* contradict the accepted notions regarding the equality of the critical exponents in continuum and lattice percolation, we merely mention this in passing until the issue can be resolved by further investigations. From now on we use the accepted lattice values of the exponent  $\gamma$  to bias the theory.

In three dimensions, up to  $\eta=0.8$ , the *greatest* discrepancy between theory and “experiment” is only 4%, well within the limits of the simulation error. Even at  $\eta=0.8$ , the largest discrepancy we have, the deviation is only about 6%, still within the simulation error (which increases slightly with  $\eta$  because of the above mentioned problems in performing the simulations in the vicinity of  $\eta=1$ ).

This trend continues in dimension 4, where the discrepancy between the theory and the simulations remains below 6% until  $\eta=0.65$ , and in dimension 5. Note, however, that as a general rule simulation errors increase with dimensionality due to the greater difficulty in performing the simulations, and therefore comparison with the theory becomes slightly more problematic. In particular, at  $D=5$  there seems to be a systematic discrepancy with the theory which could well reflect some finite size scaling effects in the simulations. It is therefore quite possible that the theory is actually more precise at this point than the simulations.

Considering that we use the series for  $S$  only up to second order, the quantitative agreement obtained is a remarkable success for the theory.

## VII. DISCUSSION

We have seen how the Potts fluid mapping allows us to derive a general expansion in powers of the density for the mean cluster size and the pair connectedness. This expansion can be used to calculate the percolation threshold by calculating the first terms in the series then using some extrapolation method to find the radius of convergence of the series. We have applied this scheme to interacting hypercubes in dimensions ranging from 2 to 7, and we have shown that even with merely three terms in the series we already obtain very good quantitative results, within a few percent of the results of the computer simulations.

Ours is not the first work to use density expansions of the mean cluster size, obtained in one way or another (e.g., from an analogy with lattice systems [26]), but we believe it is the first one to derive quantitatively adequate results for interacting systems. We believe this success stems from a simple but fundamental reason.

When Coniglio, DeAngelis, and Forlani [8] obtained their expansion of  $S$ , they did not use it directly to calculate the critical density. Instead, they turned for inspiration to the theory of liquids and considered the integral equations for the pair correlation which had proved successful there, primarily the Percus-Yevick (PY) equation. Coniglio, DeAngelis, and Forlani derived a percolative analog of this equation by applying the CDF algorithm to its diagrammatic expansion. Some time later, De Simone, Stratt, and Demoulini [10] applied this equation to a system of extended spheres, the spherical analog of the system investigated in the present work. The results were qualitatively correct but quantita-

tively poor. Discrepancies between theory and simulations ranged from 40% to no less than 10%. Several researchers [11] extended this work to other interactions or shapes with always the same quantitatively inadequate results. We believe this failure holds a simple (in hindsight, in fact, obvious), but apparently underappreciated lesson.

The guiding principle behind the work of Coniglio, DeAngelis, and Forlani and their followers seems to have been viewing continuum percolation as a high-density phenomenon. This is very reasonable from a point of view which starts from the usual theory of fluids and then extracts the percolative quantities from their normal fluid analogs. The CDF algorithm is explicitly based on this point of view; given, e.g., the direct correlation function  $c_f(\vec{r})$  of the fluid, the percolating part  $c^+(\vec{r})$  can be extracted from it by looking at a diagrammatic expansion. This means we need to know  $c_f(\vec{r})$  first. The percolation transition occurs at relatively high densities, so that the normal fluid is either a dense gas or a liquid. In this case, integral equations are the main tool for calculating the fluid's properties, and therefore an adequate starting point for obtaining the percolative properties as well.

But such a point of view misses the most important aspect of the percolation transition, namely, that it *is* a phase transition. Integral equations are known to describe the liquid well only away from the liquid-gas critical point. As we approach the transition, they fail. The quantitative failure of the percolative integral equations suggests that they suffer from an analogous defect. There is direct evidence for this claim. Seaton and Glandt [27] checked the mean cluster size for a wide range of densities and compared the predictions of integral equations with the simulations. They found that the integral equations are indeed very successful away from the critical density, but worsen steadily as  $\rho \rightarrow \rho_c$ . In short, the percolative integral equations behave with respect to the percolation transition exactly as their analogs in liquids behave with respect to the liquid transition.

At first sight this seems puzzling. At  $\rho_c$ , the normal liquid is usually away from its own critical point, and it *is* therefore well described by integral equations. Now the procedure for extracting the percolative part from these equations involves *no further approximations*. Why, then, do we obtain a relatively bad approximation by extracting *exactly* the percolative part from a very *good* approximation?

This is precisely the heart of the matter, which is the trivial observation that the phase transition is entirely ruled by the *singular* part of the relevant functions. Integral equations tend to smooth out this singular part, as evidenced, for example, by their systematic overestimation of the critical density [10]. This does not matter for the description of the liquid, because the singular part is small at these densities. However, when we turn to the percolative analog, the entire physics we are after lies precisely in this overly smoothed out singular part.

To understand a singular behavior, we must use methods adapted to singular functions. This is the simple but underappreciated lesson from all the preceding. It requires us to abandon the view of continuum percolation as primarily a high-density process. The density at which the transition takes place is irrelevant for the choice of descriptive tools, since it only influences the *analytical* part of the function.

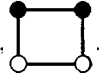
The proper tools to describe the percolation transition are not those which describe high-density systems well, but rather those which describe other phase transitions well.

The present work proceeds clearly from this point of view. The underlying normal liquid plays no part in the description presented here. Nowhere does the function  $c_f(\vec{r})$  or any of its parents appear. Instead, we have a mapping onto a Potts fluid, from which we calculate all the relevant quantities. One important difference between this and the older point of view is that the magnetic transition of the Potts fluid can be *identified* with the percolation transition, since the two relevant order parameters are essentially the same. Therefore we are forced from the outset to employ only methods which are useful for the description of the magnetic phase transition. Indeed, integral equations are not a natural tool to use here since they will clearly fail in the description of the Potts fluid. Instead, we rely on one of the best tried methods in critical phenomena, namely, an expansion valid in the disordered phase (high temperature usually, low density in the present case). A low-density expansion makes no sense from the point of view of percolation as a high-density phenomenon. Indeed, we do not expect the actual value of  $S$  obtained from the truncated series to be even remotely good. But what we look for is a failure of convergence, the appearance of a singularity, and for this a truncated series can be singularly well adapted, as shown repeatedly by countless investigations of the Ising model [19] and, even more relevantly, of percolation on a lattice [28]. More examples and applications can also be found in Ref. [29].

It is precisely because the mapping onto a Potts fluid identifies one phase transition (percolation) with another (magnetic) that we can achieve a remarkable *quantitative* agreement between theory and simulations. Clearly, the truncated series expansion coupled with an extrapolation method to find the radius of convergence is at present the best available method to calculate theoretically the critical density in continuum percolation.

## APPENDIX

We consider some diagram in the expansion, e.g., the ex-

ample used in Sec. IV, . On this diagram we define

a bond-percolation problem. We can now map the problem onto a spin model by simply assigning to every vertex an  $s$  spin, and assigning to every bond between the vertices  $i$  and  $j$  a function  $\phi(i, j)$  defined as in Eq. (3.1). We now proceed to show, just as in paper I, that the bond-percolation model corresponds quantitatively to the spin model. The result is again a geometrical mapping according to which every percolation configuration corresponds to several spin configurations, in each of which all the spins belonging to a single cluster are parallel. Different clusters, however, have randomly assigned spin values. The following derivation parallels closely the one presented in paper I for the continuum case.

Let the chosen diagram contain  $n$  vertices, and let us denote

$$\Gamma(1,2,\dots,n) = \prod_{\substack{\text{all existing} \\ \text{bonds in} \\ \text{the graph}}} \phi(i,j). \quad (\text{A1})$$

By convention, the two white circles are always labeled 1 and 2. The value associated with the diagram in the spin model is therefore  $\sum_{\lambda_3, \lambda_4, \dots, \lambda_n} \Gamma(1, \dots, n)$ , where we assume that the spins of the two white circles,  $\lambda_1$  and  $\lambda_2$ , are fixed, and where we ignore the integration as in Sec. IV. The integration can be restored at the very end of the proof without changing anything. For example, for the four-vertex graph mentioned above, we have

$$\Gamma(1,2,3,4) = \phi(1,3)\phi(3,4)\phi(4,2)\phi(2,1). \quad (\text{A2})$$

Let us now select two spins, say  $\lambda_i$  and  $\lambda_j$ , such that the bond  $\phi(i,j)$  exists in the graph. In the expression for  $\Gamma(1, \dots, n)$ , let us separate all possible configurations  $\{\lambda_m\}$  into those where  $\lambda_i = \lambda_j$  and the rest. Then,

$$\begin{aligned} \sum_{\lambda_m} \Gamma(1, \dots, n) &= f(i,j) \sum_{\substack{\lambda_m \\ \lambda_i = \lambda_j}} \frac{\Gamma(1, \dots, n)}{\phi(i,j)} \\ &+ f^*(i,j) \sum_{\substack{\lambda_m \\ \lambda_i \neq \lambda_j}} \frac{\Gamma(1, \dots, n)}{\phi(i,j)}. \end{aligned} \quad (\text{A3})$$

We can rewrite the sum over the spins when  $\lambda_i \neq \lambda_j$  as the difference between the sum over the spins without constraints and the sum over the spins when  $\lambda_i = \lambda_j$ , so that

$$\begin{aligned} \sum_{\lambda_m} \Gamma(1, \dots, n) &= f^\dagger(i,j) \sum_{\substack{\lambda_m \\ \lambda_i = \lambda_j}} \frac{\Gamma(1, \dots, n)}{\phi(i,j)} \\ &+ f^*(i,j) \sum_{\{\lambda_m\}} \frac{\Gamma(1, \dots, n)}{\phi(i,j)}, \end{aligned} \quad (\text{A4})$$

where we used the relation  $f^\dagger(i,j) = f(i,j) - f^*(i,j)$ . The last sum  $\sum_{\{\lambda_m\}}$  on the right hand side is now performed over all spin configurations without constraints. Let us now choose another pair of spins, say  $\lambda_i$  and  $\lambda_k$  (if such a bond exists). Repeating the previous procedure, we obtain that

$$\begin{aligned} \sum_{\lambda_m} \Gamma(1, \dots, n) &= f^\dagger(i,j) f^\dagger(i,k) \sum_{\substack{\lambda_m \\ \lambda_i = \lambda_j = \lambda_k}} \frac{\Gamma(1, \dots, n)}{\phi(i,j)\phi(i,k)} \\ &+ f^\dagger(i,j) f^*(i,k) \sum_{\substack{\lambda_m \\ \lambda_i = \lambda_j}} \frac{\Gamma(1, \dots, n)}{\phi(i,j)\phi(i,k)} \\ &+ f^*(i,j) f^\dagger(i,k) \sum_{\substack{\lambda_m \\ \lambda_i = \lambda_k}} \frac{\Gamma(1, \dots, n)}{\phi(i,j)\phi(i,k)} \\ &+ f^*(i,j) f^*(i,k) \sum_{\{\lambda_m\}} \frac{\Gamma(1, \dots, n)}{\phi(i,j)\phi(i,k)}. \end{aligned} \quad (\text{A5})$$

This argument can be easily generalized to all pairs of spins. Let us consider one of the sums into which the function  $\sum_{\lambda_m} \Gamma(1, \dots, n)$  has been decomposed a step before, and consider a pair  $(m,n)$  such that the bond  $\phi(m,n)$  exists in the chosen diagram. Two possibilities arise.

(1) Previous constraints already determine that  $\lambda_m = \lambda_n$  (for example, there could be some  $p$  for which  $\lambda_m = \lambda_p$  and  $\lambda_n = \lambda_p$ ). Then,

$$\begin{aligned} \sum_{\substack{\lambda_m \\ \text{previous} \\ \text{constraints}}} \frac{\Gamma(1, \dots, n)}{\phi(i,j) \cdots \phi(l,k)} \\ &= f^\dagger(m,n) \sum_{\substack{\lambda_m \\ \text{previous} \\ \text{constraints}}} \frac{\Gamma(1, \dots, n)}{\phi(i,j) \cdots \phi(l,k) \phi(m,n)} \\ &+ f^*(m,n) \sum_{\substack{\lambda_m \\ \text{previous} \\ \text{constraints}}} \frac{\Gamma(1, \dots, n)}{\phi(i,j) \cdots \phi(l,k) \phi(m,n)}, \end{aligned} \quad (\text{A6})$$

where we have used the fact that if  $\lambda_m = \lambda_n$ , then  $\phi(m,n) = f^\dagger(m,n) + f^*(m,n)$ .

(2) Previous constraints do not determine that  $\lambda_m = \lambda_n$ . Then the situation is as it was for the pair  $(i,j)$ , and the sum will split in the following way:

$$\begin{aligned} \sum_{\substack{\lambda_m \\ \text{constraints}}} \frac{\Gamma(1, \dots, n)}{\phi(i,j) \cdots \phi(l,k)} \\ &= f^\dagger(m,n) \sum_{\substack{\lambda_m, \dots \\ \lambda_m = \lambda_n}} \frac{\Gamma(1, \dots, n)}{\phi(i,j) \cdots \phi(l,k) \phi(m,n)} \\ &+ f^*(m,n) \sum_{\{\lambda_m, \dots\}} \frac{\Gamma(1, \dots, n)}{\phi(i,j) \cdots \phi(l,k) \phi(m,n)}, \end{aligned} \quad (\text{A7})$$

where in the second term on the right hand side no new constraint has been introduced.

The geometrical mapping follows because in case (2), every time a factor  $f^\dagger$  appears, we have a new constraint forcing the two spins to be parallel. On the other hand, in the percolation model, such a factor implies that the two vertices are connected, and therefore belong to the same cluster. When a factor  $f^*$  appears, no new constraint is added, so that the two vertices can be assigned spins at random. In case (1), on the other hand, the two spins are already forced to be parallel by virtue of some previous constraints. According to the foregoing argument, this means that they are both connected (at least indirectly) to some other spin and therefore that they already belong to the same cluster. In this case it does not matter anymore whether these vertices are also linked directly (a factor  $f^\dagger$ ) or not (a factor  $f^*$ ). Hence, we see that vertices which belong to the same cluster in the percolation picture must be assigned parallel spins while the clusters themselves have randomly assigned spin values.

When all pairs have been covered, the set of constraints of a particular sum specifies exactly which particles belong to which clusters in the original bond-percolation model configuration. Since the expression for  $\sum_{\lambda_m} \Gamma(1, \dots, n)$  contains sums over all possible constraints, it can be rewritten as a sum over all possible clusterings of the original percolation configuration. Thus let us define

$$P(\text{conn}) \equiv \prod_{\left\{ \begin{smallmatrix} \text{all} \\ \text{bound} \\ \text{pairs} \\ (i,j) \end{smallmatrix} \right\}} f^\dagger(i,j) \prod_{\left\{ \begin{smallmatrix} \text{all} \\ \text{unbound} \\ \text{pairs} \\ (m,n) \end{smallmatrix} \right\}} f^*(m,n). \quad (\text{A8})$$

Then we can write that

$$\sum_{\lambda_m} \Gamma(1, \dots, n) = \sum_{\left\{ \begin{smallmatrix} \text{all possible} \\ \text{connectivity} \\ \text{states} \end{smallmatrix} \right\}} \sum_{\left\{ \begin{smallmatrix} \lambda_m \text{ consistent} \\ \text{with the} \\ \text{connectivity} \\ \text{state} \end{smallmatrix} \right\}} P(\text{conn}), \quad (\text{A9})$$

where the sum over all spins is consistent with the connectivity state in the sense of the geometrical mapping, i.e., that all vertices within a single cluster must be assigned the same spin.

If we now assume that two vertices are connected with an unnormalized probability  $f^\dagger$  and disconnected with an unnormalized probability  $f^*$  (see Sec. IV), we have the interpretation that  $P(\text{conn})$  is the unnormalized probability of finding a specific percolation configuration of connected and disconnected vertices. Therefore, given a function  $F(1, \dots, n)$  defined in the percolation model, of the coordinates of the vertices, we can define its “average” as

$$\langle F(1, \dots, n) \rangle_p = \sum_{\left\{ \begin{smallmatrix} \text{conn} \\ \text{states} \end{smallmatrix} \right\}} P(\text{conn}) F(1, \dots, n). \quad (\text{A10})$$

Similarly, we can have averages performed in the spin model, which will be denoted by  $\langle \rangle_s$ . Given a quantity  $G$  defined in the spin model, we have

$$\langle G(1, \lambda_1; \dots; n, \lambda_n) \rangle_s = \sum_{\{\lambda_m\}} G(1, \lambda_1; \dots; n, \lambda_n) \prod_{i>j} \phi(i, j). \quad (\text{A11})$$

Note that  $\lambda_1$  and  $\lambda_2$  are assumed fixed. Equation (A9) now implies that in general, for any quantity  $G(1, \lambda_1; \dots; n, \lambda_n)$  defined in the spin model, we have that

$$\langle G(1, \lambda_1; \dots; n, \lambda_n) \rangle_s = \left\langle \sum_{\{\lambda_m: \text{cl}\}} G(1, \lambda_1; \dots; n, \lambda_n) \right\rangle_p, \quad (\text{A12})$$

where  $\sum_{\{\lambda_m: \text{cl}\}}$  means a summation over all spin configurations which are consistent with a given clustering in the sense of the geometrical mapping (i.e., such that all the spins in a single cluster are parallel).

This fundamental relation allows us to relate to each other quantities in the percolation model and quantities in the spin model. In particular, let us consider the function  $\Omega(i, j)$  defined in the percolation model as

$$\Omega(i, j) = \begin{cases} 1 & \text{if } i, j \text{ belong to the same cluster} \\ 0 & \text{otherwise.} \end{cases} \quad (\text{A13})$$

If we now denote  $P_{\text{cl}}(1, 2)$  the probability that the two white circles labeled 1 and 2 belong to the same cluster, then

$$P_{\text{cl}}(1, 2) = \langle \Omega(1, 2) \rangle_p. \quad (\text{A14})$$

We shall now prove that

$$\langle \Omega(1, 2) \rangle_p = \lim_{s \rightarrow 1} \left\langle \frac{1}{s-1} \sum_{\lambda_1, \lambda_2} \psi(\lambda_1) \psi(\lambda_2) \right\rangle_s, \quad (\text{A15})$$

where  $\psi(\lambda)$  equals  $(s-1)$  if  $\lambda=1$  and  $-1$  otherwise [see Eq. (1.3)].

By using the fundamental relation Eq. (A12), we have

$$\begin{aligned} & \left\langle \frac{1}{s-1} \sum_{\lambda_1, \lambda_2} \psi(\lambda_1) \psi(\lambda_2) \right\rangle_s \\ &= \left\langle \frac{1}{s-1} \sum_{\{\lambda_m: \text{cl}\}} \sum_{\lambda_1, \lambda_2} \psi(\lambda_1) \psi(\lambda_2) \right\rangle_p. \end{aligned} \quad (\text{A16})$$

We now separate the average on the right hand side into two parts: when  $\lambda_1$  and  $\lambda_2$  belong to the same cluster and when they do not. Then, from the definition of the percolation average, Eq. (A10),

$$\begin{aligned} & \left\langle \sum_{\{\lambda_m: \text{cl}\}} \sum_{\lambda_1, \lambda_2} \psi(\lambda_1) \psi(\lambda_2) \right\rangle_p \\ &= \sum_{\left\{ \begin{smallmatrix} \text{conn} \\ \text{states} \end{smallmatrix} \right\}} P(\text{conn}) \sum_{\{\lambda_m: \text{cl}\}} \sum_{\lambda_1, \lambda_2} \psi(\lambda_1) \psi(\lambda_2) \Omega(1, 2) \\ &+ \sum_{\left\{ \begin{smallmatrix} \text{conn} \\ \text{states} \end{smallmatrix} \right\}} P(\text{conn}) \sum_{\{\lambda_m: \text{cl}\}} \sum_{\lambda_1, \lambda_2} \psi(\lambda_1) \psi(\lambda_2) \\ &\times [1 - \Omega(1, 2)]. \end{aligned} \quad (\text{A17})$$

The first sum contributes only if  $\lambda_1, \lambda_2$  belong to the same cluster, while the second contributes only if they belong to separate clusters. Because of the geometrical mapping,  $\psi(\lambda_1) = \psi(\lambda_2)$  in the first sum. Also, in the sum over  $\{\lambda_m: \text{cl}\}$ , every cluster other than the one containing  $\lambda_1$  and  $\lambda_2$  contributes a factor  $s$ , the number of possible spin assignments. The cluster containing  $\lambda_1$  and  $\lambda_2$ , on the other hand, contributes a factor  $(s-1)^2$  if  $\lambda_1 = \lambda_2 = 1$  and  $(-1)^2$  for the  $(s-1)$  other possible choices for  $\lambda_1 = \lambda_2$ . Therefore

$$\begin{aligned} & \sum_{\{\lambda_m: \text{cl}\}} \sum_{\lambda_1, \lambda_2} \psi(\lambda_1) \psi(\lambda_2) \Omega(1, 2) \\ &= s^{K-1} [(s-1)^2 + (s-1)(-1)^2] \Omega(1, 2), \end{aligned} \quad (\text{A18})$$

where  $K$  is the total number of clusters in the configuration. Hence,

$$\begin{aligned}
& \sum_{\{\text{conn states}\}} \frac{P(\text{conn})}{s-1} \sum_{\{\lambda_m: \text{cl}\}} \sum_{\lambda_1, \lambda_2} \psi(\lambda_1) \psi(\lambda_2) \Omega(1,2) \\
&= \sum_{\{\text{conn states}\}} P(\text{conn}) s^{K-1} (s-1+1) \Omega(1,2) \\
&= \langle s^K \Omega(\lambda_1, \lambda_2) \rangle_p. \quad (\text{A19})
\end{aligned}$$

The second term on the right hand side of Eq. (A17) contributes only if  $\lambda_1, \lambda_2$  belong to different clusters. The cluster containing  $\lambda_1$  contributes a factor  $(s-1)$  if  $\lambda_1=1$ , and a factor  $(-1)$  in all the other  $(s-1)$  cases. The same holds for the cluster containing  $\lambda_2$ . The  $K-2$  remaining clusters each contribute a factor  $s$ . Since the values of  $\lambda_1$  and  $\lambda_2$  are assigned independently of each other, we have that

$$\begin{aligned}
& \sum_{\{\lambda_m: \text{cl}\}} \sum_{\lambda_1, \lambda_2} \psi(\lambda_1) \psi(\lambda_2) [1 - \Omega(1,2)] \\
&= s^{K-2} [(s-1) + (s-1)(-1)]^2 [1 - \Omega(1,2)] = 0. \quad (\text{A20})
\end{aligned}$$

Combining Eqs. (A19) and (A20), we see that

$$\lim_{s \rightarrow 1} \left\langle \frac{1}{s-1} \sum_{\lambda_1, \lambda_2} \psi(\lambda_1) \psi(\lambda_2) \right\rangle_s = \langle \Omega(1,2) \rangle_p. \quad (\text{A21})$$

Now, separating the case  $\lambda_1 = \lambda_2 \equiv \sigma$  from the case  $\lambda_1 \equiv \sigma \neq \lambda_2 \equiv \xi$ , we have that

$$\begin{aligned}
\left\langle \sum_{\lambda_1, \lambda_2} \psi(\lambda_1) \psi(\lambda_2) \right\rangle_s &= \sum_{\sigma} \psi^2(\sigma) R(\sigma, \sigma) \\
&+ \sum_{\sigma \neq \xi} \psi(\sigma) \psi(\xi) R(\sigma, \xi), \quad (\text{A22})
\end{aligned}$$

where

$$R(\lambda_1, \lambda_2) \equiv \sum_{\lambda_3, \dots, \lambda_n} \Gamma(\lambda_1, \lambda_2, \lambda_3, \dots, \lambda_n), \quad (\text{A23})$$

in which we have written explicitly the spin variables in the function  $\Gamma(1,2,\dots,n)$  for clarity. It is important to see that because of the summation over  $\lambda_3, \dots, \lambda_n$ ,  $R(\lambda_1, \lambda_2)$  is independent of the specific value of  $\lambda_1$  and  $\lambda_2$ , and depends only on whether they are equal. Because of this, we now have that

$$\begin{aligned}
& \sum_{\sigma} \psi^2(\sigma) R(\sigma, \sigma) = (s-1)^2 R(\alpha=1, \alpha=1) + (s-1) \\
& \times (-1)^2 R(\sigma=\alpha, \sigma=\alpha), \quad (\text{A24})
\end{aligned}$$

where  $\alpha$  is some arbitrary value of the spin different from 1. The factor  $(s-1)$  in the last term on the right hand side represents the possible choices of this spin  $\alpha \neq 1$ . As a result,

$$\lim_{s \rightarrow 1} \frac{1}{s-1} \sum_{\sigma} \psi^2(\sigma) R(\sigma, \sigma) = \lim_{s \rightarrow 1} R(\alpha, \alpha), \quad (\text{A25})$$

where  $\alpha \neq 1$ , but is otherwise arbitrary.

Similarly,

$$\begin{aligned}
& \sum_{\sigma \neq \xi} \psi(\sigma) \psi(\xi) R(\sigma, \xi) = (s-1)^2 [R(1, \alpha) + R(\alpha, 1)] \\
& + (s-1)(s-2) R(\alpha, \eta), \quad (\text{A26})
\end{aligned}$$

where  $\alpha \neq \eta$  are arbitrary values of the spin which are both different from 1. As a result,

$$\lim_{s \rightarrow 1} \frac{1}{s-1} \sum_{\sigma \neq \xi} \psi(\sigma) \psi(\xi) R(\sigma, \xi) = - \lim_{s \rightarrow 1} R(\alpha, \eta). \quad (\text{A27})$$

Combining Eqs. (A25) and (A27) we have that

$$\lim_{s \rightarrow 1} \left\langle \frac{1}{s-1} \sum_{\lambda_1, \lambda_2} \psi(\lambda_1) \psi(\lambda_2) \right\rangle_s = \lim_{s \rightarrow 1} [R(\alpha, \alpha) - R(\alpha, \eta)], \quad (\text{A28})$$

where  $\alpha, \eta \neq 1$  and  $\alpha \neq \eta$ . Comparing with Eqs. (A14), (A21), and (A23), we finally obtain that

$$\begin{aligned}
P_{\text{cl}}(1,2) &= \lim_{s \rightarrow 1} \left[ \sum_{\lambda_3, \dots, \lambda_n} \Gamma(\alpha, \alpha, \lambda_3, \dots, \lambda_n) \right. \\
&\quad \left. - \sum_{\lambda_3, \dots, \lambda_n} \Gamma(\alpha, \eta, \lambda_3, \dots, \lambda_n) \right]. \quad (\text{A29})
\end{aligned}$$

For the specific example of the four-vertex graph mentioned at the beginning of this section, for example, this means that

$$P_{\text{cl}}(1,2) = \text{CDF} \left[ \begin{array}{c} \bullet \cdots \bullet \\ \vdots \quad \vdots \\ \circ \cdots \circ \end{array} \right] = \lim_{s \rightarrow 1} \left[ \begin{array}{c} \bullet \quad \bullet \\ \alpha \quad \alpha \end{array} - \begin{array}{c} \bullet \quad \bullet \\ \alpha \quad \eta \end{array} \right]. \quad (\text{A30})$$

This clearly holds for all the diagrams in the CDF expansion. If we restore the integration on the black circles, we find that this proves the equivalence, diagram by diagram, of the CDF algorithm and the expansion we derived in the present paper.



- [1] A. Drory, Phys. Rev. E **54**, 5992 (1996); **54**, 6003 (1996).
- [2] For a review, see I. Balberg, Philos. Mag. B **55**, 991 (1987).
- [3] S. A. Safran, I. Webman, and G. S. Grest, Phys. Rev. A **32**, 506 (1985); A. L. R. Bug, S. A. Safran, G. S. Grest, and I. Webman, Phys. Rev. Lett. **55**, 1896 (1985).
- [4] G. Deutscher, in *Disordered Systems and Localization*, edited by C. Castellani, C. Di Castro, and L. Peliti (Springer-Verlag, Berlin, 1981).
- [5] J. Texeira, in *Correlations and Connectivity*, edited by H. E. Stanley and N. Ostrowsky (Kluwer, Dordrecht, 1990).
- [6] A. Okazaki, K. Maruyama, K. Okumura, Y. Hasegawa, and S. Miyazama, Phys. Rev. E **54**, 3389 (1996).
- [7] I. Balberg, C. H. Anderson, S. Alexander, and N. Wagner, Phys. Rev. B **30**, 3933 (1984).
- [8] A. Coniglio, U. DeAngelis, and A. Forlani, J. Phys. A **10**, 1123 (1977).
- [9] J. P. Hansen and I. R. McDonald, *Theory of Simple Liquids*, 2nd ed. (Academic, London, 1986).
- [10] T. De Simone, R. M. Strat, and S. Demoulini, Phys. Rev. Lett. **56**, 1140 (1986); T. De Simone, S. Demoulini, and R. M. Strat, J. Chem. Phys. **85**, 391 (1986).
- [11] Y. C. Chiew and E. D. Glandt, J. Phys. A **16**, 2599 (1983); S. C. Netemeyer and E. D. Glandt, J. Chem. Phys. **85**, 6054 (1986).
- [12] U. Alon, A. Drory, and I. Balberg, Phys. Rev. A **42**, 4634 (1990).
- [13] A. Drory, I. Balberg, U. Alon, and B. Berkowitz, Phys. Rev. A **43**, 6604 (1991).
- [14] W. Klein, Phys. Rev. B **26**, 2677 (1982).
- [15] J. A. Given, J. Chem. Phys. **90**, 5068 (1989).
- [16] J. A. Given and W. Klein, J. Chem. Phys. **90**, 1116 (1989).
- [17] J. A. Given and G. Stell, Physica A **161**, 152 (1989); J. Stat. Phys. **59**, 981 (1990).
- [18] A. Drory, Phys. Rev. E **55**, 3878 (1997).
- [19] H. E. Stanley, *Introduction to Phase Transitions and Critical Phenomena* (Oxford University, New York, 1971).
- [20] D. S. Gaunt and A. J. Guttmann, in *Phase Transitions and Critical Phenomena*, edited by C. Domb and M. S. Green (Academic, London, 1974), Vol. 3.
- [21] See, for example, *Handbook of Mathematical Functions*, edited by M. Abramovitz and I. A. Stegun (Dover, New York, 1968), p. 15.
- [22] G. A. Arteca, F. M. Fernandez, and E. A. Castro, Phys. Rev. A **33**, 1297 (1986).
- [23] A. Drory, B. Berkowitz, and I. Balberg, Phys. Rev. E **49**, R949 (1994); **52**, 4482 (1995).
- [24] D. Stauffer and A. Aharony, *Introduction to Percolation Theory*, 2nd revised ed. (Taylor and Francis, London, 1994).
- [25] H. J. Herrmann and D. Stauffer, Z. Phys. B **44**, 339 (1981).
- [26] W. Haan and R. Zwanzig, J. Phys. A **10**, 1547 (1977).
- [27] N. A. Seaton and E. D. Glandt, J. Chem. Phys. **86**, 4668 (1987); **87**, 1785 (1987).
- [28] J. W. Essam and M. F. Sykes, J. Math. Phys. (N.Y.) **7**, 1573 (1966); J. W. Essam, *ibid.* **12**, 874 (1971); in *Phase Transitions and Critical Phenomena*, edited by C. Domb and M. S. Green (Academic, London, 1972), Vol. 2.
- [29] J. Adler, Y. Meir, A. Aharony, A. B. Harris, and L. Klein, J. Stat. Phys. **58**, 511 (1990).